Continuous-time image reconstruction for binary tomography

Yusaku Yamaguchi[1], **Ken'ichi Fujimoto**[2],
Omar M. Abou Al-Ola[3], **Tetsuya Yoshinaga**[2]

[1]Graduate School of Health Sciences, The University of Tokushima
[2]Institute of Health Biosciences, The University of Tokushima
[3]Faculty of Science, Tanta University
[1,2]3-18-15 Kuramoto, Tokushima 770-8509, Japan
[3]El-Giesh St., Tanta, Gharbia, Egypt

E-mail: yamaguchi@x.medsci.tokushima-u.ac.jp,
fujimoto@medsci.tokushima-u.ac.jp, omar26_7@yahoo.com,
yosinaga@medsci.tokushima-u.ac.jp

Abstract. Binary tomography is the process of reconstructing a binary image from a finite number of projections. We present a novel method for solving binary tomographic inverse problems using a continuous-time image reconstruction (CIR) system described by nonlinear differential equations based on the minimization of a double Kullback-Leibler divergence. We prove theoretically that the divergence measure monotonically decreases in time. Moreover, we demonstrate numerically that the quality of the reconstructed images of the nonlinear CIR system is better than those from an iterative reconstruction method.

Keywords: Binary tomography; Continuous-time image reconstruction; Differential equation; Stability of solution; Kullback-Leibler divergence

1. Introduction

Binary tomography is concerned with the reconstruction of a binary image from a finite number of projections [1, 2]. In contrast to continuous tomography which is used in, e.g., medical X-ray computed tomography (CT) and nuclear emission CT, binary tomography focuses on the problem of locating an object such as a tumor or blood vessel in the human body by means of X-ray CT. This kind of inverse problem can be reduced to a convex, box-constrained optimization problem. As iterative algorithms for solving the problem, a spectral projected gradient (SPG) method [3, 4] and binary steering of a non-binary iterative method [5, 6] have been presented. On the other hand, in this paper, we propose a new approach to reconstructing binary tomographic images resulting from the idea of continuous dynamical methods [7, 8, 9, 10, 11, 12, 13]. It consists of a continuous-time image reconstruction (CIR) system described by a piecewise-smooth switched differential equation based on the minimization of a double Kullback-Leibler

(KL) divergence. Because all solutions to the nonlinear differential equation stay within the constrained subspace corresponding to the domain of the divergence, the CIR system is well-defined if an initial value is taken in the subspace. We prove theoretically that the double KL-divergence measure can be a common Lyapunov function [14] for the CIR system. This means that the measure monotonically decreases along the solution to the switched differential equation for arbitrary switching signals [15, 16]. Moreover, we compare numerically the convergence properties of the nonlinear CIR method with those of the maximum-likelihood expectation-maximization (ML-EM) method, which is a well-known iterative reconstruction technique for emission CT. We show that CIR has an advantage in terms of the distance to the actual solution under the same measure observed via the projection data, and the quality of reconstructed images of the CIR is better than those of the iterative reconstruction algorithm.

2. System Description

Let $x \in \bar{\Omega} \subset R^J$ be an unknown variable for pixel values satisfying

$$y = Ax \tag{1}$$

where $y \in R_+^I$ and $A \in R_+^{I \times J}$ denote the projection value and a normalized projection operator corresponding to the Radon transform, respectively, with R_+ denoting the set of non-negative real numbers. We say that the system $y = Ax$ is consistent if it has a solution. Equation (1) is an ill-posed problem if its solution is not unique or does not exist [17]. The binary reconstruction problem is to find a binarization of x from an optimization minimizing an appropriate cost function $V(x)$ regarding the linear system in Eq. (1) with $\bar{\Omega}$ being the closure of the open hypercube $\Omega = (0, 1)^J$.

Before defining the cost function for the inverse problem, we introduce the generalized Kullback-Leibler divergence [18] of two non-negative vectors α and β:

$$\mathrm{KL}(\alpha, \beta) = \sum_{\ell} \beta_\ell \log \frac{\beta_\ell}{\alpha_\ell} + \alpha_\ell - \beta_\ell \tag{2}$$

where α_ℓ and β_ℓ denote the ℓth elements of α and β, respectively. The divergence $\mathrm{KL}(\alpha, \beta)$ for the vectors α and β of non-negative real numbers is non-negative with $\mathrm{KL}(\alpha, \beta) = 0$ if and only if $\alpha = \beta$. This divergence is also called Csiszár's I-divergence measure [19]. It leads to effective selection methods for solving optimization problems with non-negativity constraints and is the only choice consistent with a set of intuitive postulates such as regularity, locality, and composition-consistency [19, 20].

To solve the inverse problem of binary tomography, we shall consider the minimization problem,

$$\min_{x(t) \in \bar{\Omega}} V(x(t)), \quad t \in R \tag{3}$$

$$\begin{aligned} V(x) &:= \mathrm{KL}(x, e) + \mathrm{KL}(u - x, u - e) \\ &= \sum_{j=1}^{J} e_j \log \frac{e_j}{x_j} + (1 - e_j) \log \frac{1 - e_j}{1 - x_j} \end{aligned}$$

where u denotes an all-ones vector $(1, 1, \ldots, 1)^\top$ of length J. Here, we assume that $e \in \{0, 1\}^J$ is a binary solution of Eq. (1) and is excluded from the vectors of all-zeros and all-ones. It is easily seen that $V(x) > 0$ unless $x = e$. If there exists a situation such that the pair (x_j, e_j) is either $(1, 0)$ or $(0, 1)$ for some j, we have $V = +\infty$. Therefore, we can say that the cost function V showing the double KL-divergence is sensitive to errors. To obtain a time evolution $x(t)$ that converges to a local minimum of the function $V(x(t))$, we formulated a switched nonlinear system consisting of the family of subsystems

$$\frac{dx}{dt} = -X(U - X){A_m}^\top(A_m x - y_m), \qquad (4)$$
$$t - k\tau \in [t_{m-1}, t_m), \quad t \in R_+, \quad x(0) = x^0$$

for a series of times $0 = t_0 < t_1 < t_2 < \ldots < t_M = \tau$ and non-negative integer k, where $X := \mathrm{diag}(x)$ indicates the diagonal matrix in which the diagonal entries starting in the upper left corner are the elements of x, and U denotes the identity matrix, while $A_m \in R_+^{I_m \times J}$ and $y_m \in R_+^{I_m}$ are, respectively, a submatrix consisting of I_m partial rows of A and a subvector of y with the same corresponding rows of A_m, for $m = 1, 2, \ldots, M$, with M denoting the total number of divisions. We see that the closed convex set $\bar{\Omega}$ is contained within the state space R^J of the solutions, and the vector field of each subsystem is sufficiently smooth with respect to the state variables.

Note that if we write the subsystem as

$$\frac{dx}{dt} = -X(U - \gamma^{-1}X){A_m}^\top(A_m x - y_m) \qquad (5)$$

with a positive parameter γ, the CIR systems for continuous tomography considered in Refs. [21, 22] and for binary tomography defined in Eq. (4) correspond to the cases where $\gamma = \infty$ and $\gamma = 1$, respectively.

3. Theoretical Analysis

In this section, we give theoretical results for the behavior of the solution to the dynamical system in Eq. (4). First, we show that all solutions stay inside the hypercube.

Proposition 1. *If we choose initial value $x^0 \in \Omega = (0, 1)^J$ in the switched dynamical system in Eq. (4), then the solution $\phi(t, x^0)$ stays in Ω for all $t \in R_+$.*

Proof. Since the subsystem can be written as $dx_j/dt = -x_j(1 - x_j)({A_m}^\top)_j(A_m x - y_m)$, we see that, on the subspace where $x_j = 0$ or $x_j = 1$, the solution satisfies $d\phi_j/dt \equiv 0$ for any j. Therefore, the subspace is invariant and trajectories cannot pass through every invariant subspace, according to the uniqueness of solutions for the initial value problem. This leads to any solution $\phi(t, x^0)$ of any subsystem in Eq. (4) with initial value $x^0 \in \Omega$ being in Ω for all $t \in R_+$. Consequently, if we choose an initial value in Ω for the first subsystem under arbitrary switching in the switched system, an end point of the corresponding trajectory, at a given time of switching, which is the initial point for the second subsystem, will be in Ω, and so on. □

Note that none of the trajectories converge to the trivial equilibria, the all-zeros and all-ones vectors, which are unexpected for image reconstruction.

Proposition 2. *The equilibria* 0 *and* u *of the dynamical system in Eq. (4) are locally unstable.*

Proof. We rewrite the subsystem in Eq. (4) as

$$\frac{dx}{dt} = f_m(x), \quad m = 1, 2, \ldots, M.$$

The derivative of f_m with respect to x is

$$\frac{\partial f_m}{\partial x}(x) = -X(U - X){A_m}^\top A_m - (U - 2X)\,\mathrm{diag}\left({A_m}^\top(A_m x - y_m)\right).$$

Therefore, the Jacobian matrices of the linearized equations at the equilibria 0 and u are respectively

$$\frac{\partial f_m}{\partial x}(0) = \mathrm{diag}({A_m}^\top y_m)$$

and

$$\frac{\partial f_m}{\partial x}(u) = \mathrm{diag}({A_m}^\top(A_m u - y_m)) = \mathrm{diag}({A_m}^\top A_m(u - e)).$$

We see that all the eigenvalues of each matrix are non-negative for any $m = 1, 2, \ldots, M$, and accordingly, both equilibria are unstable. □

Next, we prove the main theoretical result concerning the stability of the common equilibrium e satisfying $y_m = A_m e$ for $m = 1, 2, \ldots, M$. Namely, the existence of a common Lyapunov function for the family of subsystems in Eq. (4) guarantees the stability of the equilibrium e in the corresponding switched system for arbitrary switching signals (see Ref. [15]).

Theorem 1. *If the system* $y = Ax$ *has a unique solution* $e \in \{0, 1\}^J$*, the common equilibrium* e *for the dynamical system corresponding to the family of systems in Eq. (4) is uniformly asymptotically stable.*

Proof. Consider a Lyapunov-candidate-function defined in the convex set $\bar{\Omega}$ as

$$V(x) = \mathrm{KL}(x, e) + \mathrm{KL}(u - x, u - e), \tag{6}$$

which is positive definite with respect to the point e, and can be written as

$$\begin{aligned} V(x) &= \sum_{j=1}^{J} e_j \log \frac{e_j}{x_j} + (1 - e_j) \log \frac{1 - e_j}{1 - x_j} \\ &= \sum_{j=1}^{J} \int_{e_j}^{x_j} \left(\frac{v - e_j}{v} + \frac{v - e_j}{1 - v} \right) dv \\ &= \sum_{j=1}^{J} \int_{e_j}^{x_j} \frac{v - e_j}{v(1 - v)} dv. \end{aligned}$$

We obtain its derivative along the solution to the subsystem in Eq. (4) as follows:

$$\begin{aligned}\left.\frac{dV}{dt}(x)\right|_{(4)} &= \sum_{j=1}^{J}\frac{x_j-e_j}{x_j(1-x_j)}\frac{dx_j}{dt} \\ &= -\sum_{j=1}^{J}(x_j-e_j)({A_m}^{\top})_j(A_mx-y_m) \\ &= -\|A_mx-y_m\|_2^2 \\ &< 0\end{aligned} \tag{7}$$

for x in Ω, which is well-defined according to Proposition 1 by choosing an initial value in Ω, and for $m = 1, 2, \ldots, M$. Moreover, the derivative is zero at $x = e \in \bar{\Omega}$. Thus, all subsystems in the family in Eq. (4) share a common Lyapunov function given by Eq. (6), and therefore, the corresponding switched system is uniformly asymptotically stable; the terminology uniform is employed here to indicate uniformity with respect to the switching signals. □

4. Experimental Results and Discussion

For ill-posed inverse problems consisting of a binary phantom image and projection data with a small number of projection views, we compared the CIR method with the ML-EM method (an iterative method). Figure 1 illustrates an 87×87 binary phantom image with only black and white pixels, which corresponds to $e \in \{0,1\}^{7569}$. Supposing 128 ray paths per projection view for the phantom image, we obtain a normalized projection operator $A \in R_+^{128p\times 7569}$, where p denotes the number of projection views. In our experiments, we considered three noise-free projection data sets that were algebraically calculated using $y = Ae$ where $y \in R_+^{128p}$ with $p = 4, 5, 6$. Therefore, each CT problem has an infinite number of solutions owing to underdetermined problems such that $I = 128p < J$. We here set the angles of projection views to $\{0°, 45°, 90°, 135°\}$ for four projection views, $\{0°, 36°, 72°, 108°, 144°\}$ for five projection views, and $\{0°, 30°, 60°, 90°, 120°, 150°\}$ for six projection views. The angles were measured counterclockwise from the vertical line that passes through the center of the phantom image.

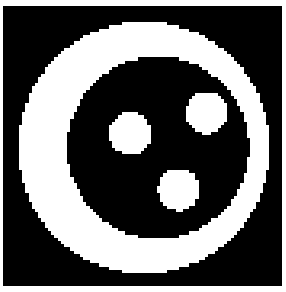

Figure 1. 87×87 binary phantom image with black and white pixels.

To simplify the comparison, we dealt with an unblocked CIR system derived from Eq. (4) with $M = 1$. Its dynamics is described by

$$\frac{dx}{dt} = -X(U - X)A^{\top}(Ax - y), \quad t \in R_{+}. \tag{8}$$

According to Proposition 1, we set the initial values to $x(0) = x^0 \in (0, 1)^J$ so that the domain of solutions to this system becomes $(0, 1)^J$. As mentioned above, this method based on Eq. (8) minimizes Eq. (6). We numerically confirmed that the KL-divergence is monotone decreasing even for the ill-posed case. On the other hand, the iterative step of the ML-EM method is defined by

$$z_j(n+1) = z_j(n)s_j^{-1}\sum_{i=1}^{I}\frac{A_{ij}y_i}{(Az(n))_i}, \quad n = 0, 1, \ldots, \quad z_j(0) = x_j^0 \tag{9}$$

for $j = 1, 2, \ldots, J$, where $s_j = \sum_{i=1}^{I} A_{ij}$ and A_{ij} is an (i, j) element of A. The ML-EM algorithm minimizes [23] the function $\mathrm{KL}(Az, y)$ over all non-negative vectors z. It converges to a solution, but no characterization of the limit is known [23]. For binary tomography, Censor [1] proposed a binary steering of the non-binary iterative method that steers the reconstruction process towards a binary solution. The steering process is a heuristic step with no deeper mathematical justification. In this paper, to seek a solution in $\bar{\Omega}$, we modify the ML-EM method by replacing the $z_j(n+1)$ given by Eq. (9) with a smaller value between one and $z_j(n + 1)$.

In order to compare the convergence properties of the continuous-time and discrete-time systems, we select the points of times with the same measure, which can be observed via the projection data. Using the solutions $x(t)$ to Eq. (4) and $z(n)$ to Eq. (9) emanating from the same initial value $x^0 \in \Omega$, the set of a pair of times is defined as

$$\begin{aligned}\Gamma := \{(n, t) \in Z_{+} \times R_{+} : {} & K(z(n)) = K(x(t)), \\ & K(z(k-1)) > K(z(k)) \text{ for } k = 1, 2, \ldots, n, \\ & K(x(\tau)) \text{ is monotonically decreasing for } \tau \in [0, t]\}\end{aligned} \tag{10}$$

with Z_{+} denoting the set of positive integer numbers and $K(w) := \mathrm{KL}(Aw, y)$. Now, let us consider the distances

$$(D_z(n), D_x(n)) := \left(\frac{\|z(n) - e\|_1}{\|e\|_1}, \frac{\|x(t) - e\|_1}{\|e\|_1}\right), \quad (n, t) \in \Gamma. \tag{11}$$

In Fig. 2, the sequences of $D_x(n)$ and $D_z(n)$ along the solutions to Eqs. (8) and (9) with initial values x^0 are plotted as solid and dotted lines. The results in Figs. 2(a), 2(b), and 2(c) were obtained from projection data sets with four, five, and six projection views, respectively. For each projection data set, the values of $D_x(n)$ and $D_z(n)$ decrease as n increases. This illustrates that the quality of images with either method becomes better and better as time passes. Moreover, $D_x(n)$ is always less than $D_z(n)$; i.e., this suggests that the CIR method produces images that are more similar to the phantom image compared with the ML-EM method. We also found that the contribution of the ML-EM method to minimize the absolute relative error for the phantom image was smaller than that of the CIR method in spite of it minimizing the value of $\mathrm{KL}(Az, y)$.

Figure 3 compares tomographic images reconstructed with the two methods. These images were reconstructed from four, five, and six projection views and from values of $D_x(n)$ and $D_z(n)$ at $n = 92$, 53, and 92, respectively; the n corresponds to the right end of the abscissa in each graph. The images were also binarized using a simple threshold technique that makes the color of the jth pixel white only if the value of the jth state variable is greater than 0.5; otherwise, the pixel is black. We also present the Hamming

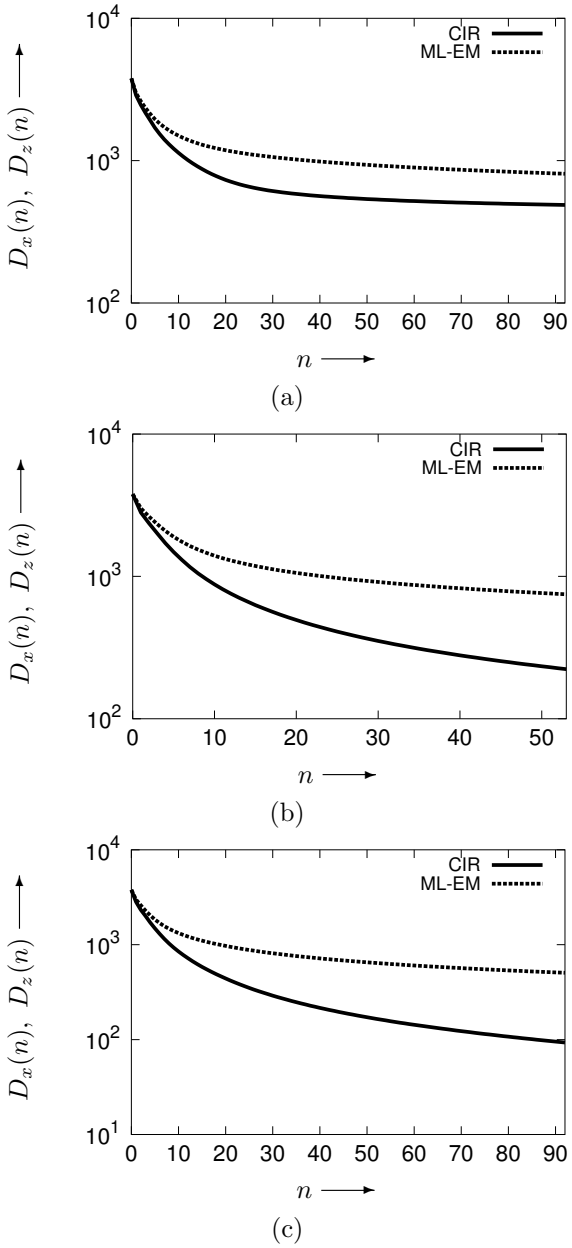

Figure 2. Comparison of CIR and ML-EM methods using sequences of absolute relative errors for phantom image. $D_x(n)$ and $D_z(n)$ corresponding to CIR and ML-EM methods are plotted as solid and dotted lines, respectively. Projection data sets had (a) four, (b) five, and (c) six projection views.

distance (H) between the binarized reconstructed image and the phantom image below each image.

A comparison of these images shows that the quality of images made with the CIR method is better than the quality of the images made with the ML-EM method at $(n, t) \in \Gamma$. The decrease in H also provides us with a quantitative evaluation for visual inspection. In particular, H was zero for the image made with the CIR method and six projection views; i.e., the reconstructed binary image and the phantom image were exactly the same.

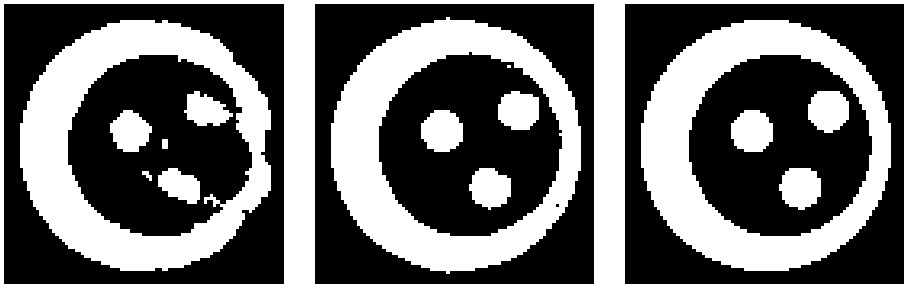

$H = 282$ $H = 61$ $H = 0$

(a)

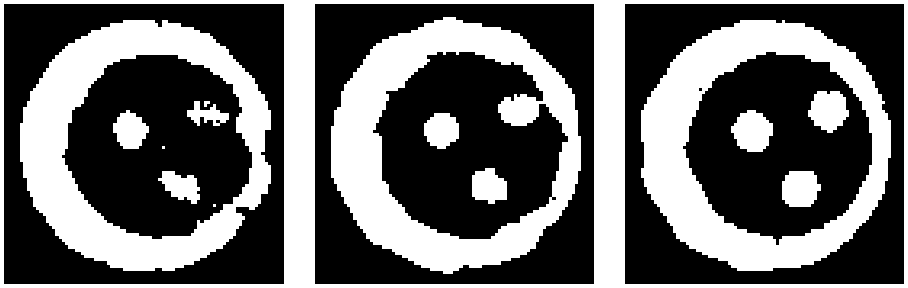

$H = 386$ $H = 343$ $H = 180$

(b)

Figure 3. Images reconstructed with (a) CIR method and (b) ML-EM method. All the images were binarized by using a thresholding technique, and the images from the left to the right were reconstructed using projection data sets with four, five, and six projection views, respectively. H denotes the Hamming distance between a binary reconstructed image and the phantom image.

5. Concluding Remarks

We proposed a nonlinear continuous method for solving inverse problems in binary tomography. The CIR system produces box-constrained solutions and in the well-posed case, convergence is theoretically guaranteed on the basis of minimization of the double KL-divergence measure. Through numerical experiments, we confirmed that the divergence measure monotonically decreases even in the ill-posed case with a small number of projection views. It is also found that $D_x(n)$ is less than $D_z(n)$ at all points of

times $(n,t) \in \Gamma$ under the same measure observed via projection data, where $D_x(n)$ and $D_z(n)$ denote the distances to the actual solution for the CIR and ML-EM methods, respectively. Moreover, we demonstrated that the images with the CIR method are higher in quality than those made with the ML-EM method. These results lead us to the conclusion that the CIR method would be effective for binary tomography.

Acknowledgments

This research is partially supported by Aihara Innovative Mathematical Modelling Project, the Japan Society for the Promotion of Science (JSPS) through its "Funding Program for World-Leading Innovative R&D on Science and Technology (FIRST Program)."

References

[1] G.T. Herman, A. Kuba, Discrete Tomography: Foundations, Algorithms, and Applications, Series: Applied and Numerical Harmonic Analysis, Birkhauser, Boston, 1999.

[2] G.T. Herman, A. Kuba, Advances in Discrete Tomography and Its Applications, Series: Applied and Numerical Harmonic Analysis, Birkhauser, Boston, 2007.

[3] E.G. Birgin, J.M. Martinez, M. Raydan, Nonmonotone spectral projected gradient methods on convex sets, SIAM J. Optimization. 10 (2000) 1196–1211.

[4] T. Lukić, A. Lukity, Binary Tomography Reconstruction Algorithm Based on the Spectral Projected Gradient Optimization, Proc. of the 10th International Symposium of Hungarian Researchers on Computational Intelligence and Informatics (2009) 253–263.

[5] Y. Censor, Binary steering in discrete tomography reconstruction with sequential and simultaneous iterative algorithms, Lin. Algebra and its Appl. 339 (2001) 111–124.

[6] K.J. Batenburg, J. Sijbers, DART: A Practical Reconstruction Algorithm for Discrete Tomography, IEEE Transactions on Image Processing. 20 (9) (2011) 2542–2553.

[7] M.K. Gavurin, Nonlinear functional equations and continuous analogies of iterative methods, Izv. Vuzov., Ser. Matematika, 5 (1958) 18—31.

[8] J. Schropp, Using dynamical systems methods to solve minimization problems, Appl. Numer. Math. 18 (1) (1995) 321–335.

[9] R.G. Airapetyan, Continuous Newton method and its modification, Applicable Analysis, 73 (3-4) (1999) 463–484.

[10] R.G. Airapetyan, A.G. Ramm, A.B. Smirnova, Continuous analog of gauss-newton method, Math. Models Meth. Appl. Sci. 9 (3) (1999) 463–474.

[11] R.G. Airapetyan, A.G. Ramm, Dynamical systems and discrete methods for solving nonlinear ill-posed problems, Appl. Math. Rev., World Sci. Pub. Co., 1 (2000) 491–536.

[12] A.G. Ramm, Dynamical systems method for solving operator equations, Commun. Nonlin. Sci. Numer. Simul. 9 (4) (2004) 383–402.

[13] L. Li, B. Han, A dynamical system method for solving nonlinear ill-posed problems, Appl. Math. Comput. 197 (1) (2008) 399–406.

[14] A.M. Lyapunov, Stability of motion, Academic Press, New York, 1966.

[15] D. Liberzon, Switching in Systems and Control, Birkhauser, Boston, 2003.

[16] H. Lin, P.J. Antsaklis, Stability and stabilizability of switched linear systems: A survey of recent results, IEEE Trans. Autom. Control. 54 (2) (2009) 308–322.

[17] J. Hadamard, Sur les problèmes aux dérivées partielles et leur signification physique, Princeton University Bulletin, Princeton University (1902).

[18] S. Kullback, R.A. Leibler, On Information and Sufficiency, Ann. Math. Stat. 22 (1) (1951) 79–86.
[19] I. Csiszár, Why least squares and maximum entropy? An axiomatic approach to inference for linear inverse problems, Ann. Stat. 19 (4) (1991) 2032–2066.
[20] D.L. Snyder, T.J. Schulz, J.A. O'Sullivan, Deblurring subject to nonnegativity constraints, IEEE Trans. Signal Process. 40 (5) (1992) 1143–1150.
[21] K. Fujimoto, O.M. Abou Al-Ola, T. Yoshinaga, Continuous-time image reconstruction using differential equations for computed tomography, Commun. Nonlinear Sci. Numer. Simulat. 15 (6) (2010) 1648–1654.
[22] O.M. Abou Al-Ola, K. Fujimoto, T. Yoshinaga, Common Lyapunov function based on Kullback-Leibler divergence for a switched nonlinear system, Mathematical Problems in Engineering. Article ID 723509 (2011).
[23] C.L. Byrne, A unified treatment of some iterative algorithms in signal processing and image reconstruction, Inverse Problems. 20 (2004) 103–120.